Journal of Catalysis 258 (2008) 324–333

Contents lists available at ScienceDirect

Journal of Catalysis

www.elsevier.com/locate/jcat

# Obtaining the best composition of supported $V_2O_5$–$MoO_3/TiO_2$ catalyst for propane ODH reaction

T.V. Malleswara Rao [a], E. Vico-Ruiz [b], M.A. Bañares [b], Goutam Deo [a,*]

[a] Department of Chemical Engineering, Indian Institute of Technology Kanpur, Kanpur 208 016, India
[b] Catalytic Spectroscopy Laboratory, Instituto de Catálisis y Petroleoquímica, CSIC, Marie Curie 2, Cantoblanco, E-28049 Madrid, Spain

ARTICLE INFO

*Article history:*
Received 12 March 2008
Revised 8 June 2008
Accepted 2 July 2008
Available online 3 August 2008

*Keywords:*
Propane
Supported
ODH
$V_2O_5$
$MoO_3$
$TiO_2$
Raman

ABSTRACT

The best composition for achieving maximum propene yields during the propane ODH reaction over supported $V_2O_5$–$MoO_3/TiO_2$ (VMoTi) catalysts were determined by applying statistical methodologies. Catalyst characterizations revealed that noninteracting surface vanadia and molybdena species exist. The kinetic parameters, apparent pre-exponential factors, and activation energies also were estimated for the propane ODH reaction over the VMoTi catalysts. Based on statistical methodologies, the maximum propene yields at iso-conversion were obtained for the catalysts containing high V and low Mo concentrations (3.42V0.6MoTi) and those containing low V and high Mo concentrations (0.6V3.42MoTi). Of the two, the 3.42V0.6MoTi catalyst is better, because it has the highest activity and provides the best propene yield at iso-conversion.



## 1. Introduction

The oxidative dehydrogenation (ODH) of propane to propene has received considerable attention in recent years because of its significant advantages over the dehydrogenation process, which is presently used for alkene production [1–5]. However, achieving high propene yields in catalytic propane oxidation is extremely challenging because the propene thus formed is further oxidized to the thermodynamically stable carbon oxides (CO and $CO_2$). Current efforts are concentrated on designing a proper catalyst that produces higher propene yields at higher conversions.

The catalytic performances of the supported and mixed vanadia-based catalysts have been widely explored for selective oxidation processes [6–20]. In particular, the propane ODH reaction has been successfully studied over $TiO_2$ and $Al_2O_3$-supported vanadia catalysts [6–17]. Studies by various research groups [17,21–28] have shown that adding secondary metal oxides (oxides of Mo, W, Sb, Li, Na, K, Bi and Cr) to the $V_2O_5/Al_2O_3$ system in propane ODH reaction increases both propene yield and selectivity. Adding alkali metals [29–31] and phosphorous [32] to the $V_2O_5/TiO_2$ system also increases propene selectivity but decreases the activity. In these studies the optimum composition of vanadia and molybdena was not determined, however.

The present work examines the performance of the supported $V_2O_5$–$MoO_3/TiO_2$ catalysts for propane ODH reaction with the aim of identifying the compositions of $V_2O_5$ and $MoO_3$ required to achieve the optimum propene yields by statistical analysis. The supported $V_2O_5$–$MoO_3/TiO_2$ (VMoTi) catalysts were prepared by the incipient wetness co-impregnation method. The synthesized catalysts were then considered for the propane ODH reaction. The compositions of $V_2O_5$ and $MoO_3$ that produced the optimum propene yield were determined by applying the factorial design of experiments and response surface methodology. The importance of these statistical approaches has not been fully realized in heterogeneous catalysis despite their powerful applications. In particular, Weckhuysen et al. [33] applied statistical methods to study the effects of various factors, including operating conditions, Cr-speciation, chromia loading, and support composition, on isobutane dehydrogenation activity over supported chromia catalysts. In the present study, kinetic analysis also was done for the optimum VMoTi catalysts to gain insight into the differences in their catalytic performance compared with the unmodified $V_2O_5/TiO_2$ catalysts.

## 2. Experimental

### 2.1. Catalyst preparation

Supported $V_2O_5$–$MoO_3TiO_2$ (VMoTi) catalysts with different V and Mo loadings were prepared by the incipient wetness co-impregnation method. The $TiO_2$ support (Degussa, P-25) was ini-

* Corresponding author. Fax: +91 512 2590104.
*E-mail address:* goutam@iitk.ac.in (G. Deo).

0021-9517/$ – see front matter 
doi:10.1016/j.jcat.2008.07.001

tially pretreated with incipient volumes of oxalic acid solution and then heat-treated. Details of the heat treatment procedure are given below. The vanadium and molybdenum oxide precursors were ammonium metavanadate ($NH_4VO_3$, Aldrich 99.99%) and ammonium heptamolybdate ($(NH_4)_6Mo_7O_{24}\cdot 4H_2O$, Aldrich, 99.98%), respectively. The co-impregnation of V and Mo ions for each sample was achieved by thorough mixing of the precursor solution containing V and Mo ions with the pretreated support. The resulting mixture was kept in a desiccator overnight, followed by drying at 383 K for 6 h and then at 473 K for another 6 h. Finally, the samples were calcined at 723 K for 6 h. The prepared catalysts are designated *x*V*y*MoTi, where *x* and *y* are the wt% loadings corresponding to $V_2O_5$ and $MoO_3$, respectively. The vanadia and molybdena loadings were chosen based on the factor levels determined by the factorial design of experiments. An unmodified $V_2O_5/TiO_2$ (VTi) catalyst also was prepared as described elsewhere [34], and its catalytic performance was compared with that of the modified catalysts.

### 2.2. Catalyst characterization

#### 2.2.1. Surface area and X-ray diffraction

The prepared samples were characterized for their surface area and analyzed by X-ray diffraction (XRD). The surface areas of the samples were obtained by the BET multipoint method using $N_2$ adsorption data at 77 K. Details of the surface area measurement are provided elsewhere [34]. Powder XRD patterns of the prepared catalysts were measured with a Seifert ISO-Debyeflex 2002 using Ni filtered $K\alpha$ radiation from a Cu target ($\lambda = 1.44056$ Å).

#### 2.2.2. In situ Raman spectroscopy

The in situ Raman spectra were obtained with a single monochromatic Renishaw Micro-Raman System 1000 equipped with a thermoelectrically cooled charge-coupled device detector (200 K) and a holographic super-Notch filter that removes the elastic scattering. The samples were excited with the 514-nm Ar line in an in situ cell (Linkam, TS-1500), which allows temperature treatments up to 1773 K under flowing gases. The spectral resolution was 3 $cm^{-1}$, and the spectrum acquisition time was 300 s for each sample. The spectra of the samples under dehydrated conditions were acquired at 573 K in dry synthetic air for 1 h. The Raman spectra were obtained using very low laser power (typically <1 mW) to ensure that no local heating occurred. The spectra of the $TiO_2$-supported samples were normalized based on the ~633 $cm^{-1}$ peak of bulk $TiO_2$ to facilitate comparison of the different samples.

#### 2.2.3. Fourier transform infrared spectroscopy

The dehydrated Fourier transform infrared (FT-IR) spectra were acquired with a Bruker TENSOR 27 spectrometer equipped with an air-cooled high-emission IR source and a low-noise DLATGS detector. The samples were placed in an in situ Harrick IR cell (HVC) with the Praying Mantis diffuse reflectance accessory, designed to perform the measurements at elevated temperatures. The IR measurements were performed at a spectral resolution of 4 $cm^{-1}$ for 128 scans. The dehydrated conditions of the samples were obtained at 673 K in dry synthetic air for 1 h. Before the spectra of the samples were obtained, the spectrum of the KBr sample was acquired and used as a reference.

#### 2.2.4. Temperature-programmed reduction using hydrogen ($H_2$-TPR)

The $H_2$-temperature-programmed reduction (TPR) studies were performed in a Micromeritics Pulse Chemisorb 2705 apparatus. A sample weight of ~0.02–0.03 g was used for reduction measurements. Details of the $H_2$-TPR measurements are given elsewhere [6].

### 2.3. Reaction studies

The prepared catalysts were evaluated for the propane oxidation reaction at atmospheric pressure in a vertical down-flow quartz reactor mounted in a tubular furnace. Details of the reactor and the experimental procedure are given elsewhere [34]. The effect of contact time on propane oxidation over the VMoTi catalysts was studied at 673 K and a propane-to-$O_2$ molar ratio of 2:1 by changing the total reactant flow rate between 45 and 120 mL/min. For kinetic parameter determination, the experiments were conducted by varying the temperature between 613 and 673 K and the propane-to-oxygen molar ratio between 3:1 and 1:1. Nitrogen was used as a diluent in all of the reaction studies, with its mole fraction in the inlet stream adjusted such that the inlet nitrogen-to-oxygen molar ratio was 0.79:0.21. A constant total flow rate of 60 mL/min was maintained. Additional details are available elsewhere [34].

Reactions were conducted in the absence of catalyst, and insignificant conversions were observed under the present experimental conditions. Low propane conversions were maintained to facilitate proper kinetic parameter estimation. For all of the catalysts, several runs were taken at a particular temperature, and the average value was considered. The standard deviation of the data was <1.0%. Based on the inlet and outlet concentrations, the activity, conversion, selectivity, and yield were calculated based on formulas given elsewhere [6]. The effects of interphase, interparticle, and intraparticle diffusion limitations were considered by applying published criteria [35]; none were found.

## 3. Process optimization

The primary objective of the present study was to determine the composition of the VMoTi catalysts to obtain the maximum propene yield at iso-conversion. The optimization study was carried out by response surface methodology (RSM) involving factorial design of experiments.

### 3.1. Response surface methodology

RSM is a very useful technique for optimizing response functions, which are RSM influenced by several variables [36–39]. In brief, the methodology is as follows. Let $Y$ be the response of a chemical process (dependent variable), which is a function of $k$ factor levels, $x_1, x_2, \ldots, x_k$ (independent variables) that can be measured quantitatively. The response function for the $u$th combination of factor levels is

$$Y_u = f(x_{1u}, x_{2u}, \ldots, x_{ku}) + \varepsilon_u, \quad u = 1, 2, \ldots, N, \tag{1}$$

where $N$ is the number of experiments and $\varepsilon$ is the noise or error involved.

A geometric representation of the response function in the region of factor levels is called a "response surface." The true functional relationship between the response and the independent variables is generally unknown, and polynomial models usually provide good approximations in relatively small regions of factor levels.

RSM involves three steps. The first step requires proper design of experiments to estimate the model parameters effectively. The factorial designs are very useful when the number of factors or independent variables is small. The second step is to approximate a suitable polynomial model to fit the experimental data and then test for model adequacy by applying the lack-of-fit F-test [37–39]. The final step is to determine the values of the factors that would produce the optimum response.

The most common polynomial models used for RSM analysis are the first-order and the quadratic, or second-order, model.

The first-order model for $k$ factors, which is applicable for flat responses, is given by

$$Y = b_0 + b_1x_1 + b_2x_2 + \cdots + b_kx_k + \varepsilon. \quad (2)$$

For responses that have curvature, a second-order model is recommended

$$Y = b_0 + \sum_{i=1}^{k} b_ix_i + \sum_{i=1}^{k} b_{ii}x_i^2 + \sum_{i}\sum_{\substack{j \\ i<j}} b_{ij}x_ix_j + \varepsilon. \quad (3)$$

The **b** parameters of the polynomial models are estimated by the least squares method.

In the present analysis, we adopted the matrix approach to solving Eqs. (2) and (3). Here **Y** is defined as an $(n \times 1)$ vector of responses; **X**, as an $(n \times p)$ matrix of independent variables; **b**, as an $(p \times 1)$ vector of parameters to be estimated; and $\boldsymbol{\varepsilon}$, as an $(n \times 1)$ vector of errors. Thus, Eq. (2) or (3) can be written in matrix form as

$$\mathbf{Y} = \mathbf{Xb} + \boldsymbol{\varepsilon}. \quad (4)$$

The least squares estimator of **b** that minimizes sum of the squares of the errors is $\hat{\mathrm{b}}$ given by

$$\hat{\mathrm{b}} = (\mathbf{X}^{\mathrm{T}}\mathbf{X})^{-1}\mathbf{X}^{\mathrm{T}}\mathbf{Y}, \quad (5)$$

where $\mathbf{X}^{\mathrm{T}}$ is the transpose of the matrix **X** and $(\mathbf{X}^{\mathrm{T}}\mathbf{X})^{-1}$ is the inverse of the matrix $(\mathbf{X}^{\mathrm{T}}\mathbf{X})$. The details of the solution by this matrix approach are given elsewhere [37,38].

### 3.2. Response and factors for propane ODH over VMoTi catalysts

The propene yield at iso-conversion was considered as the response, $Y$, to be optimized with respect to the factors influencing the propane oxidation process. The factors of interest chosen were wt% loadings of vanadia and molybdena on the titania support, represented by V and Mo, respectively. The propene yields were obtained from the contact time studies of propane oxidation over the VMoTi catalysts at 2.5% propane conversion. The contact time studies were carried out at 673 K and a propane-to-oxygen ratio of 2:1.

### 3.3. Levels and coding of factor levels for $2^2$ factorial design of experiments

Initially, a $2^n$ factorial design (where $n$ is the number of factors and each run is at two levels) with two factors was considered for the analysis to study the influence of the factors (V and Mo) on propene yield. In the $2^2$ design, the levels of the factors are generally called "lower" and "upper" levels and coded as $(-1)$ and $(+1)$, respectively. The levels of the factors (V and Mo) were chosen such that the total V + Mo coverage was less than the (V + Mo) monolayer coverage. The monolayer coverage for the supported VTi and MoTi catalysts reportedly corresponds to 7–9 V atoms/nm$^2$ [7,40–43] and 5–6 Mo atoms/nm$^2$ [44,45], respectively. Based on the surface area of titania (45 m$^2$/g) used in the present study, the foregoing monolayer values correspond to 6 wt% vanadia and 6 wt% molybdena, respectively. Thus, the (V + Mo) monolayer capacity was assumed to be 6 wt% of (V + Mo) oxide on the titania support. The two factors were coded for convenience as follows:

$$x_{\mathrm{V}} = \frac{\mathrm{V} - \left(\frac{\mathrm{V_{lower}} + \mathrm{V_{upper}}}{2}\right)}{\left(\frac{\mathrm{V_{upper}} - \mathrm{V_{lower}}}{2}\right)} \quad (6)$$

and

$$x_{\mathrm{Mo}} = \frac{\mathrm{Mo} - \left(\frac{\mathrm{Mo_{lower}} + \mathrm{Mo_{upper}}}{2}\right)}{\left(\frac{\mathrm{Mo_{upper}} - \mathrm{Mo_{lower}}}{2}\right)}, \quad (7)$$

**Table 1**
Experimental matrix for the central composite design

| Run | V (wt%) | Mo (wt%) | $x_{\mathrm{V}}$ | $x_{\mathrm{Mo}}$ | $Y_P$ (%) |
|---|---|---|---|---|---|
| 1 | 1 | 1 | −1 | −1 | 1.800 |
| 2 | 3 | 1 | +1 | −1 | 1.986 |
| 3 | 1 | 3 | −1 | +1 | 1.993 |
| 4 | 3 | 3 | +1 | +1 | 1.830 |
| 5 | 2 | 2 | 0 | 0 | 1.950 |
| 6 | 2 | 2 | 0 | 0 | 1.935 |
| 7 | 2 | 2 | 0 | 0 | 1.947 |
| 8 | 2 | 2 | 0 | 0 | 1.937 |
| 9 | 3.414 | 2 | 1.414 | 0 | 1.900 |
| 10 | 0.586 | 2 | −1.414 | 0 | 1.918 |
| 11 | 2 | 3.414 | 0 | 1.414 | 1.890 |
| 12 | 2 | 0.586 | 0 | −1.414 | 1.924 |

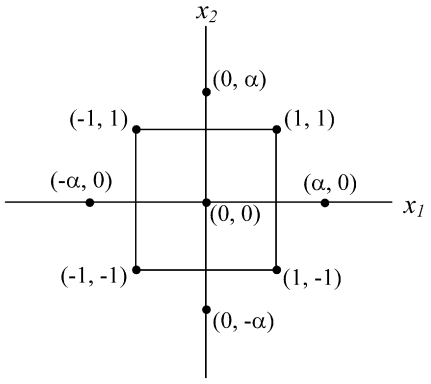


**Fig. 1.** Central composite design for two factors.

where V and Mo are the actual or natural variables representing the loadings of vanadia and molybdena, respectively; "lower" and "upper" subscripts of the V and Mo indicate the lower and upper limits of the respective variables; and $x_{\mathrm{V}}$ and $x_{\mathrm{Mo}}$ are the coded variables for V and Mo, respectively.

### 3.4. Experimental design and model fitting

The experimental design matrix is described in Table 1. Columns 2–5 give the natural and coded levels of the two factors. The last column gives the values of the propene yield ($Y_P$) obtained at 2.5% propane conversion for each run. The first four rows correspond to $2^2$ factorial design; the next four rows are the additional runs conducted at the center point (coded as 0). These additional runs are needed to estimate the pure error and the overall curvature effect. The order in which the experiments were performed was randomized to avoid systematic errors.

To determine the interactions between the factors, initially a polynomial model given by Eq. (2) involving the main factors and interaction term was fitted to the $2^2$ design data with four replicated runs at the center point (meaning the first 8 rows in Table 1). Analysis of variance (ANOVA) was used to analyze the response function for adequacy. If a significant curvature was observed, then a full second-order model given by Eq. (3) was recommended. The second-order model would require four additional axial points (the last 4 rows in Table 1) to the initial $2^2$ design with a center point as shown in Fig. 1. The axial points are usually called "star" points, and the resulting design is called a central composite design (CCD). The fitted response equation was then used to determine the V and Mo loadings that would produce optimum propene yield.

## 4. Kinetic parameter estimation

The methodology for estimating the kinetic parameters has been described previously [6,32]. Previous studies have shown that

direct propane combustion to carbon oxides makes only a minor contribution to the propane ODH over supported vanadium oxide catalysts [46–48]. Consequently, the kinetics of the propane ODH reaction for the present study can be represented by a Mars–van Krevelen (MvK) model built on a consecutive reaction scheme. The MvK mechanism chosen for this study assumes that the propane molecules react with lattice oxygen of the catalyst to produce propene molecules ($r_1$), which then react with lattice oxygen to produce CO ($r_2$) and $CO_2$ ($r_3$). The gas-phase oxygen replenishes the lattice oxygen by reoxidation of the reduced catalyst ($r_4$).

The rate equations for the four reactions $r_1$ to $r_4$ are expressed as

$$r_1 = k_1 P_{C_3H_8}(1-\beta), \tag{8}$$

$$r_2 = k_2 P_{C_3H_6}(1-\beta), \tag{9}$$

$$r_3 = k_3 P_{C_3H_6}(1-\beta), \tag{10}$$

and

$$r_4 = k_4 P_{O_2}\beta, \tag{11}$$

where $\beta$ is the degree of reduction and is the fraction of reduced sites to the total number of sites present. According to the MvK reaction model, the rate of lattice oxygen consumed in the reactions $r_1$ to $r_3$ equals the rate of lattice oxygen replacement by the reaction $r_4$. Based on the stoichiometry, $\beta$ is expressed as

$$\beta = \frac{0.5k_1 P_{C_3H_8} + 3.0k_2 P_{C_3H_6} + 4.5k_3 P_{C_3H_6}}{0.5k_1 P_{C_3H_8} + 3.0k_2 P_{C_3H_6} + 4.5k_3 P_{C_3H_6} + k_4 P_{O_2}}. \tag{12}$$

Reparameterization is needed to facilitate proper determination of kinetic parameters [6,32,34]. Consequently, the rate constant is given by

$$k_i = k_{i0}\exp\left(\frac{-E_i}{R}\left(\frac{1}{T}-\frac{1}{T_m}\right)\right), \quad i = 1\text{–}4. \tag{13}$$

Furthermore, standard error calculations of the kinetic parameters ($k_{i0}$'s and $E_i$'s), the apparent pre-exponential factors, and activation energies were achieved by applying previously defined equations [32].

## 5. Results and discussion

### 5.1. Surface area and XRD

The surface areas of pure titania and the supported VMoTi catalysts varied between 43 and 49 $m^2/g$ of catalyst. The similar surface areas of the samples suggest that the support was not significantly affected during catalyst preparation. The powder X-ray diffractograms for all of the VMoTi catalysts (not shown for the sake of brevity) revealed the patterns of $TiO_2$ support, with no peaks due to crystalline compounds of $V_2O_5$ or $MoO_3$ or mixed V–Mo–O phases.

### 5.2. In situ Raman spectroscopy

The Raman spectra of the dehydrated titania-supported catalysts presented in Fig. 2 show the effect of molybdenum oxide on the structures of surface vanadium oxide species. The figure also shows Raman spectra of the unmodified 2VTi and 2MoTi catalysts for comparison. The 2VTi sample exhibited a sharp Raman band at ~1028 $cm^{-1}$ due to the terminal V=O bond vibration of surface isolated and polymeric vanadia species and the broad band at ~926 $cm^{-1}$ due either to V–O–Ti bond vibrations or to V–O–V bonds in polymeric vanadia species [49–51]. In contrast, the 2MoTi sample exhibited a single band at ~990 $cm^{-1}$, which is characteristic of the terminal Mo=O bond vibration of surface molybdena species [49,50]. The spectra of the modified VMoTi samples

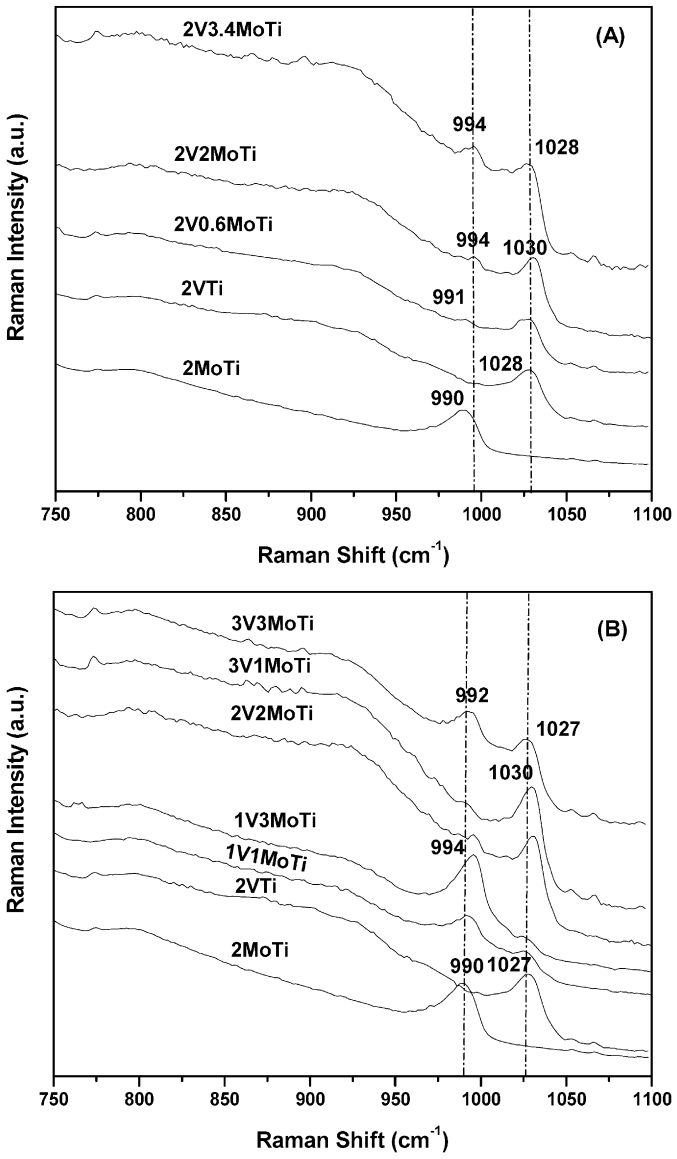


**Fig. 2.** (A) Effect of molybdenum oxide addition on Raman spectra of dehydrated VTi sample. (B) Raman spectra of dehydrated VMoTi samples corresponding to the $2^2$ factorial design.

in Fig. 2 exhibited Raman bands due to terminal Mo=O (990–994 $cm^{-1}$) and V=O (1028–1030 $cm^{-1}$) bond vibrations, similar to those observed for unmodified samples [50]. Furthermore, the observed variation in Raman band shift is within the experimental resolution of the Raman system. Fig. 2 also shows that the VMoTi samples with high vanadia content had a broad Raman feature at ~927 $cm^{-1}$, which has been assigned to the V–O–Ti bond vibrations [50,51].

Consequently, it appears that the structures of dispersed surface vanadia and molybdena species present in the VMoTi samples were affected only by an increase in the degree of polymerization. Furthermore, none of the samples exhibited the bands ascribed to the crystalline $V_2O_5/MoO_3$ and mixed V–Mo–O phases, which have been observed on supported $V_2O_5$–$MoO_3/Al_2O_3$ catalysts at high surface (V + Mo) coverages [24–26,52].

### 5.3. FT-IR spectroscopy

Fig. 3 presents the FT-IR spectra of the titania-supported catalysts under dehydrated conditions in the first overtone region

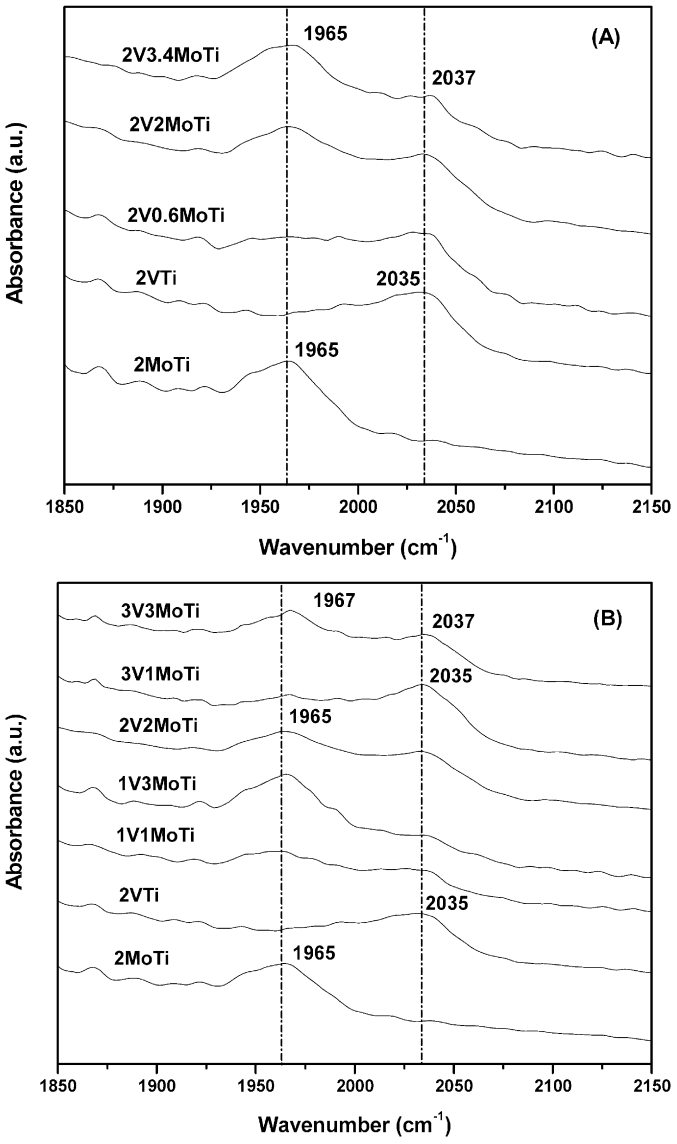


**Fig. 3.** (A) Effect of molybdenum oxide addition on FT-IR spectra of dehydrated VTi sample. (B) FT-IR spectra of dehydrated VMoTi samples corresponding to the $2^2$ factorial design.

(1850–2150 $cm^{-1}$) of M=O (M–V, Mo) stretching modes. The unmodified 2VTi catalyst has a single IR band at ~2035 $cm^{-1}$ due to the first overtone of V=O stretching [53,54]. The spectrum of the 2MoTi catalyst also showed a single band at ~1965 $cm^{-1}$, ascribed to the first overtone of Mo=O stretching [55]. Fig. 3A shows that the VMoTi samples exhibited the same IR bands corresponding to M=O (M: V, Mo) stretchings present on single-component catalysts [56,57]. With an increase in molybdena loading on 2VTi catalyst, the intensity of the IR band due to the Mo=O stretching increased, and the band position remained unchanged (~1965 $cm^{-1}$). Fig. 3B further confirms that higher (V + Mo) loadings on titania support also had the same IR bands with shape and band positions unaffected, suggesting the noninteracting nature (i.e., not reacting with each other) of the dispersed surface vanadia and molybdena species on the titania support. These IR results for the VMoTi samples also are consistent with the Raman bands observed at ~1028 $cm^{-1}$ (IR-2035 $cm^{-1}$) due to V=O stretching and at ~990 $cm^{-1}$ (IR-1965 $cm^{-1}$) due to Mo=O stretching.

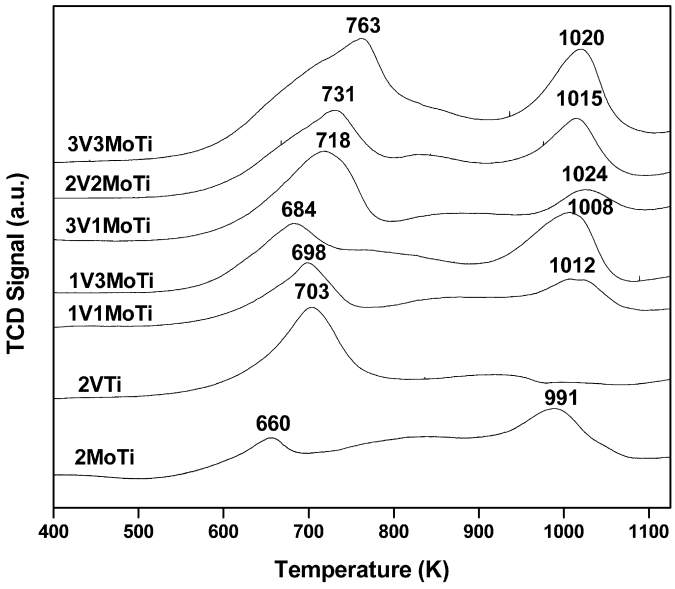


**Fig. 4.** TPR profiles of the $V_2O_5$–$MoO_3/TiO_2$, $V_2O_5/TiO_2$ and $MoO_3/TiO_2$ catalysts.

### 5.4. $H_2$-TPR

Fig. 4 presents $H_2$-TPR profiles of the VMoTi catalysts, along with the reduction measurements over supported 2% $V_2O_5/TiO_2$ (VTi) and 2% $MoO_3/TiO_2$ (MoTi) catalysts for comparison. A single reduction peak can be seen for the 2VTi sample at 400–1100 K due to the reduction of $V^{+5}$ to $V^{+3}$ [6]. In contrast, the 2MoTi sample was reduced in two steps; the lower and higher temperature peaks represent the reduction of $Mo^{+6}$ to $Mo^{+4}$ and of $Mo^{+4}$ to $Mo^{+0}$, respectively [58,59]. Furthermore, the maximum of the reduction peak ($T_{max}$) of the 2MoTi sample (660 K) was smaller than that of the 2VTi sample (703 K), suggesting that the surface molybdenum oxide species were more easily reducible in hydrogen than the surface vanadia species on the titania support.

An analysis of the TPR data for the supported VMoTi catalysts given in Fig. 4 reveals two reduction peaks. The $T_{max}$ values of the VMoTi samples suggest that the samples' reduction behavior was not significantly affected by the presence of the secondary metal oxide species; however, for the 3V3MoTi sample, the lower temperature peak at 685–720 K shifted to 763 K. This type of shift toward higher temperature was reported previously for the supported $V_2O_5/TiO_2$ catalysts with increasing vanadia loadings [47]. Quantitative analysis of the TPR results revealed that the extent of reduction nearly corresponded to the loadings of the two metal oxides. Thus, it appears that the addition of Mo had no effect on the structure of V and did not significantly affect its reducibility. The higher temperature reduction peak for all of the VMoTi samples indicates the reduction of $Mo^{+4}$ to $Mo^{+0}$ [58,59].

### 5.5. Contact time studies

Propane oxidation was initially carried out at 673 K and a $C_3H_8$-to-$O_2$ molar ratio of 2:1 as a function of contact time over the VMoTi catalysts chosen based on the design of experiments (addressed later). A 2VTi sample also was considered as a reference. An increase in propane conversion with increasing contact time was observed for all of the catalysts. Furthermore, the specific variation of propene selectivity with propane conversion over these catalysts indicates that propene was a primary product and that propene selectivity decreased with increasing propane conversion. The specific variation of CO and $CO_2$ selectivities with conversion also suggests that the carbon oxides were secondary products formed by the combustion of propene. For brevity, the contact time data are not shown.

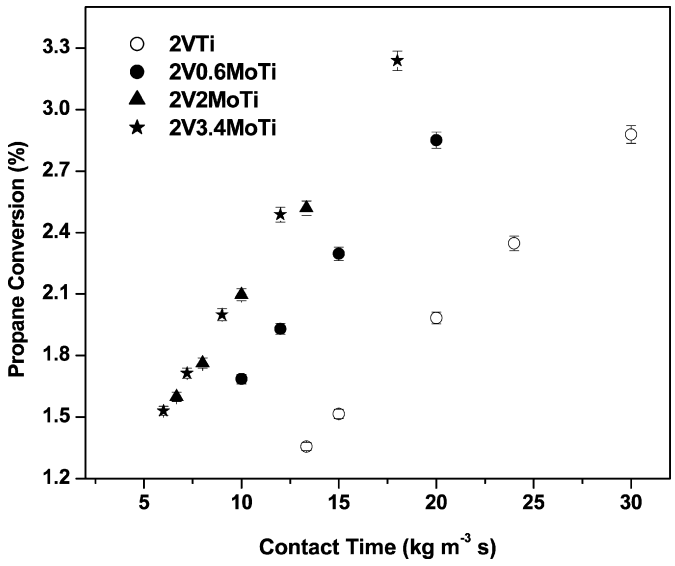


**Fig. 5.** Propane conversion as a function of contact time. At $T = 673$ K and $C_3H_8{:}O_2 = 2{:}1$.

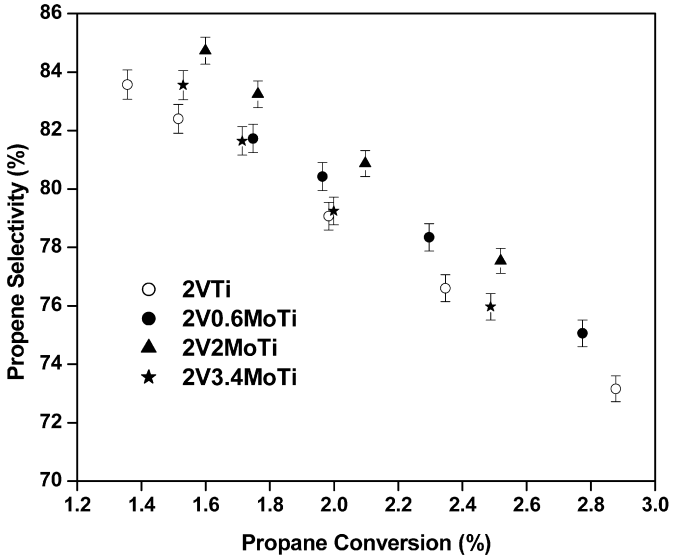


**Fig. 6.** Variation of propene selectivity with propane conversion. At $T = 673$ K and $C_3H_8{:}O_2 = 2{:}1$.

The promotional effect of molybdenum oxide on the $V_2O_5/TiO_2$ catalysts can be confirmed by comparing the reaction data for the 2VTi, 2V0.6MoTi, 2V2MoTi, and 2V3.4MoTi samples, as shown in Fig. 5. Relative to vanadia, the molybdena species was inactive; however, the presence of the molybdena species in the VMoTi samples resulted in an increase in conversion relative to the 2VTi sample. Specifically, at iso-contact time, propane conversion followed the trend 2V3.4MoTi ∼ 2V2MoTi > 2V0.6MoTi > 2VTi. From Fig. 6, the propene selectivity trend of these four catalysts was 2V2MoTi > 2V0.6MoTi > 2V3.4MoTi ∼ 2VTi. It appears that the presence of certain amounts of molybdena did lead to promotion; however, the presence of molybdena beyond this amount was detrimental to the selectivity of the VMoTi catalyst. Thus, the presence of molybdena has some promotional effect over the VTi catalyst in terms of increases in activity and propene yield for the propane oxidation reaction.

**Table 2**
ANOVA for the central composite design

| Source | SS | DF | MS | $F_o$ | $F_{\upsilon_1,\upsilon_2,0.05}$ |
|---|---|---|---|---|---|
| Regression $(x_V, x_{Mo}, x_V^2, x_{Mo}^2, x_V x_{Mo})$ | 0.0342 | 5 | 0.00684 | 28.74 | 4.39 |
| Residual | 0.00143 | 6 | $2.38 \times 10^{-4}$ | | |
| Lack of fit | 0.00127 | 3 | $4.23 \times 10^{-4}$ | 7.76 | 9.28 |
| Pure error | $1.63 \times 10^{-4}$ | 3 | $5.43 \times 10^{-5}$ | | |
| Total | 0.0356 | 11 | | | |

SS—sum of the squares. DF—degrees of freedom. MS—mean sum of the squares. $F_o$—F-ratio observed or calculated. $F_{\upsilon_1,\upsilon_2,0.05}$—F-statistical value at 95% confidence level. $\upsilon_1$, $\upsilon_2$—degrees of freedom corresponding to the numerator and denominator, respectively.

### 5.6. Response surface analysis

The propene yield ($Y_P$) at 2.5% propane conversion for each catalyst obtained from the foregoing contact study was taken as the response to be optimized with respect to the vanadia and molybdena loadings on titania support for RSM analysis. Initially, the $2^2$ experimental design coded data with center points were fitted with a polynomial (first-order) model involving propene yield ($Y_P$) and the main factors ($X_V$ and $X_{Mo}$) and interaction term ($X_V X_{Mo}$). Then ANOVA was carried out to check the statistical significance of the model. The data indicated a significant curvature effect, suggesting that the first-order model was inadequate. Thus, the first order was not an adequate approximation to represent the propene yield.

To obtain a better representation of the reaction, a more rigorous design (e.g., CCD) can be developed by adding four additional runs, called star points (coded as $\pm\alpha$) to the initial $2^2$ factorial design plus the center point (see Fig. 1). All of the data points are made to fit a full second-order model given by Eq. (3). The distance of the star points from the design center is denoted by $\alpha$; usually, $\alpha = 1.414$ for two-factor analysis [37,38]. Table 1 presents the experimental design matrix corresponding to a CCD design along with the propene yield data.

The fitted second-order propene yield model in two factors ($X_V$ and $X_{Mo}$) for CCD design-coded data is given by

$$Y_P = 1.94225 - 0.00031X_V - 0.00138X_{Mo} - 0.01807X_V^2 - 0.01907X_{Mo}^2 - 0.08725(X_V X_{Mo}). \quad (14)$$

The coefficients of the foregoing model were estimated by the method of least squares [37,38]. Table 2 presents the ANOVA data for Eq. (14). The table shows that the regression was significant (i.e., regression coefficients are important) and that the lack-of-fit was not significant, because the F-ratio calculated for regression was greater than the F-statistic value, whereas the F-ratio of lack of fit to pure error was less than the F-statistic value at a 95% confidence level. This shows that the foregoing second-order model is an adequate approximation of the propene yield and thus is appropriate for further analysis.

Using Eqs. (6) and (7), the foregoing propene yield function in actual variables is represented by

$$Y_P = 1.44807 + 0.24647\mathrm{V} + 0.2494\mathrm{Mo} - 0.01807\mathrm{V}^2 - 0.01907\mathrm{Mo}^2 - 0.08725(\mathrm{VMo}), \quad (15)$$

where V and Mo indicate the wt% loadings of vanadia and molybdena, respectively. Equation (15) was further explored to determine the optimum vanadia and molybdena concentrations to produce the optimum propene yield.

### 5.7. Determination of optimum conditions of V and Mo

Before characterizing Eq. (15), the stationary point, (V, Mo), was obtained for Eq. (15) by equating the derivative of $Y_P$ with respect

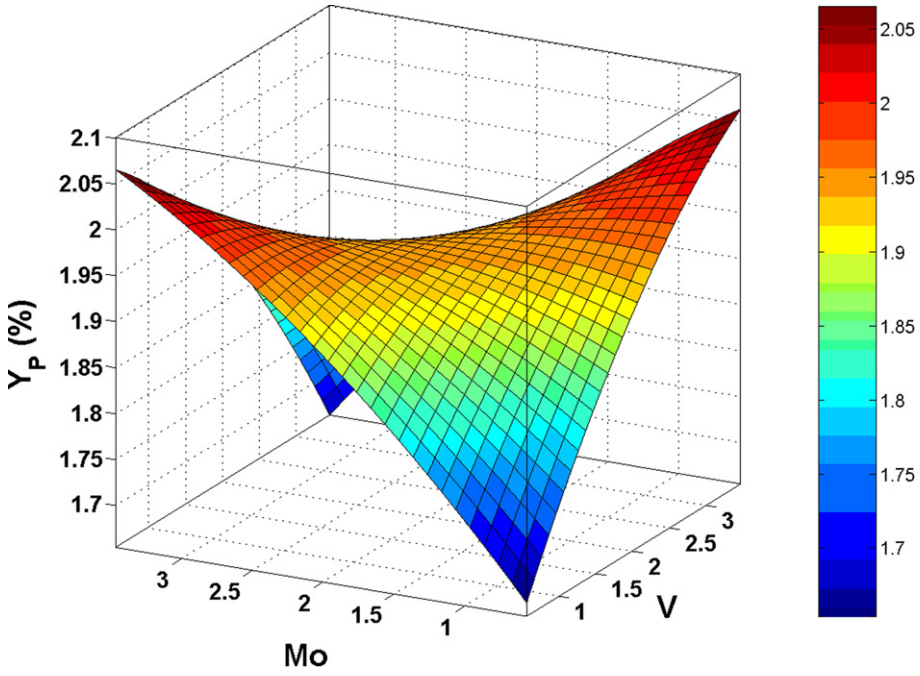


**Fig. 7.** Propene yield surface in two factors (V and Mo).

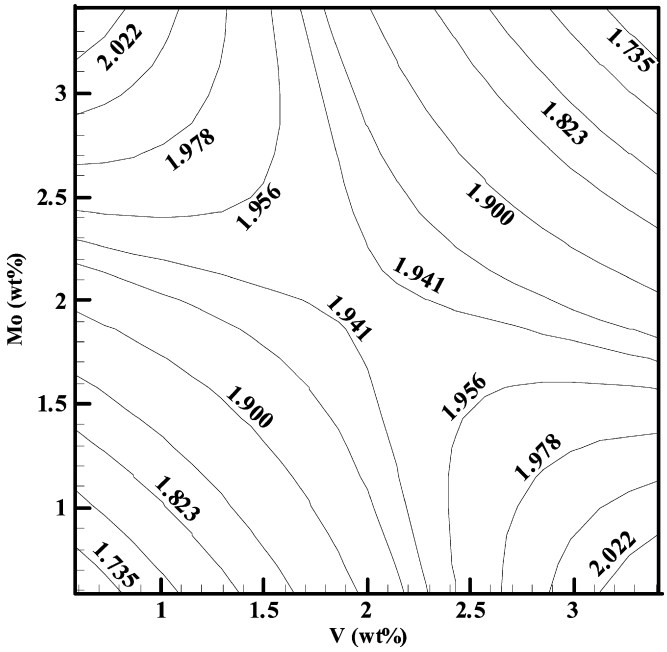


**Fig. 8.** Contour plot of the propene yield.

to the factors (V and Mo) to zero. The stationary point, (V, Mo), obtained was (2, 2), which is essentially the design center. This could represent a point of minimum or maximum propene yield or a saddle point.

To determine the nature of the stationary point, the quadratic propene yield function given by Eq. (15) is represented as a 3D response surface in Fig. 7, with the corresponding 2D contour plot shown in Fig. 8. Examining Figs. 7 and 8 reveals a saddle point or a minimax, indicating that the propene yield can increase or decrease from the center of the region, depending on the direction of movement from the center. Figs. 7 and 8 also suggest that the maximum propene yields were obtained for the VMoTi catalysts containing the highest V and lowest Mo concentrations and those containing the lowest V and highest Mo concentrations on the titania support. The highest propene yield was observed for an optimum composition of (V, Mo) ∼ (3.414, 0.586), followed by (0.586, 3.414), in the region considered. These two catalysts are designated 3.42V0.6MoTi and 0.6V3.42MoTi, respectively.

**Table 3**
Kinetic parameters for supported VMoTi and VTi catalysts

| Parameters | Units | Parameter values | | | |
|---|---|---|---|---|---|
| | | 3.42V0.6MoTi | 0.6V3.42MoTi | 2V2MoTi | 2VTi |
| $k_{10}$ | (mL STP min$^{-1}$ (g cat)$^{-1}$ atm$^{-1}$) | 127 (1) | 24 (0.5) | 75 (1) | 41 (1) |
| $k_{20}$ | | 1118 (6) | 200 (2) | 754 (6) | 605 (7) |
| $k_{30}$ | | 678 (7) | 162 (1) | 490 (2) | 399 (8) |
| $k_{40}$ | | 1556 (7) | 385 (2) | 1936 (12) | 376 (3) |
| $\frac{k_{10}}{k_{20}+k_{30}}$ | | 0.071 | 0.066 | 0.060 | 0.041 |
| $E_1$ | (kJ mol$^{-1}$) | 64 (1) | 62 (1) | 68 (1) | 71 (1) |
| $E_2$ | | 46 (2) | 52 (1) | 53 (2) | 41 (1) |
| $E_3$ | | 31 (1) | 32 (1) | 37 (2) | 27 (1) |
| $E_4$ | | 119 (2) | 223 (2) | 159 (3) | 124 (2) |
| $E_1-(E_2+E_3)/2$ | | 25.5 | 20 | 23 | 37 |

The standard errors are given in parentheses. $T_m = 643$ K.

The foregoing optimum catalysts, along with design center catalyst 2V2MoTi, were considered for kinetic analysis. The 2VTi reactivity data for propane oxidation also was considered in the kinetic analysis, to allow comparison of the catalytic performance with that of a modified 2V2MoTi catalyst.

### 5.8. Kinetic analysis

The kinetic parameters were estimated for a consecutive Mars–van Krevelen reaction model over the optimum catalysts

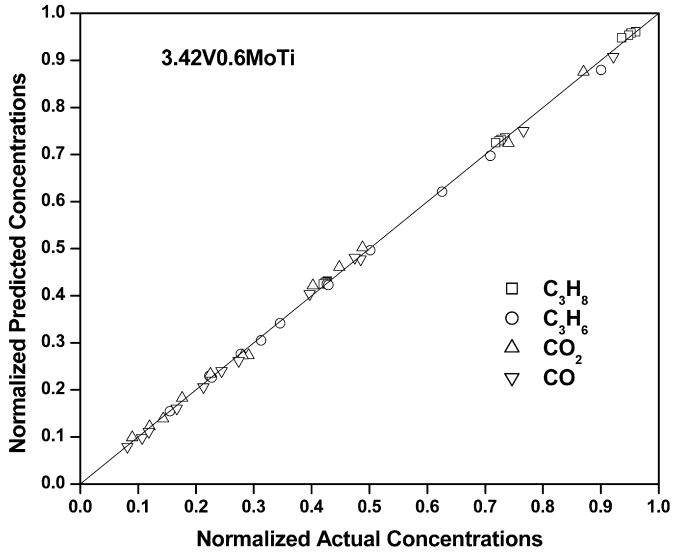


**Fig. 9.** Parity plot for 3.42V0.6MoTi catalyst.

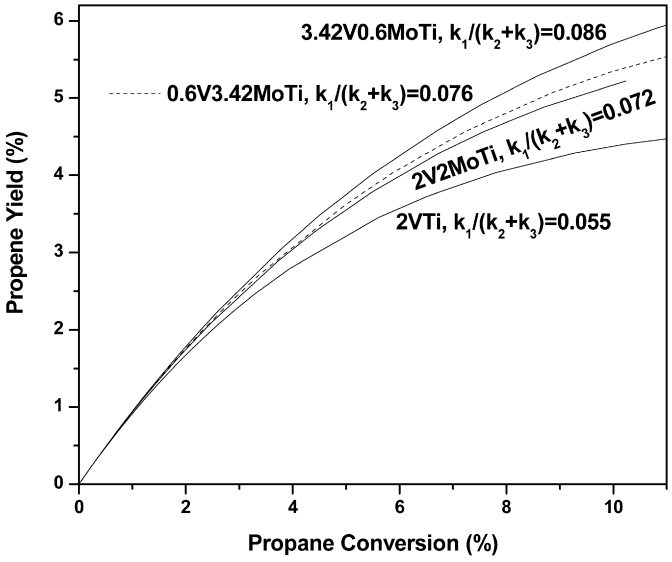


**Fig. 10.** Variation of propene yield with the propane conversion for different catalysts. At $T = 673$ K and $C_3H_8{:}O_2 = 2{:}1$.

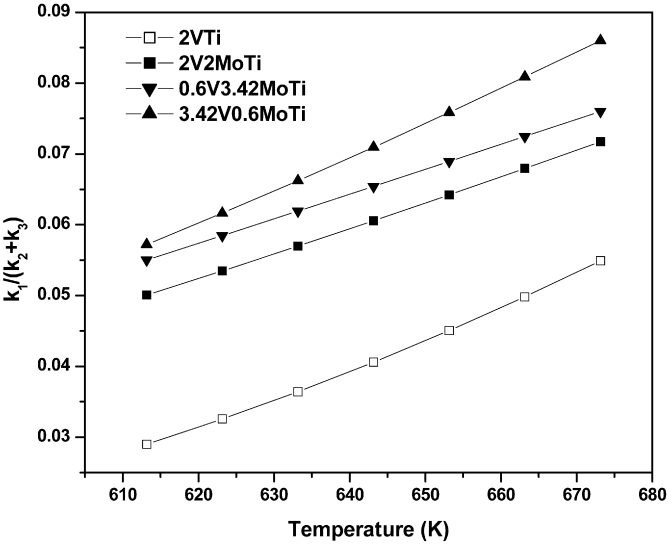


**Fig. 11.** Variation of the $k_1/(k_2 + k_3)$ ratio with temperature for different catalysts.

(3.42V0.6MoTi and 0.6V3.42MoTi), as well as the design center catalyst (2V2MoTi), to characterize the differences in the VMoTi catalysts. Table 3 gives the estimated parameter values, $k_{i0}$ and $E_i$. Based on the estimated parameters, the predicted concentrations of the carbon compounds analyzed ($C_3H_8$, $C_3H_6$, $CO_2$, and CO) were determined and compared with the actual concentrations for the 3.42V0.6MoTi catalyst given in Fig. 9. The close correspondence of these concentrations suggests that proper representation of the propane oxidation reaction over the catalysts was achieved with the estimated parameters.

The analysis of the kinetic parameters reported in Table 3 reveals that the apparent pre-exponential factors for propene formation ($k_{10}$) and propene combustion ($k_{20}$ and $k_{30}$) followed the trend 3.42V0.6MoTi > 2V2MoTi > 0.6V3.42MoTi. Comparing the activation energies of the different VMoTi catalysts reveals that the activation energy for propene formation, $E_1$, remained relatively constant at 62–68 kJ/mol. The activation energies for propene combustion reactions, $E_2$ and $E_3$, also remained relatively constant at 46–53 and 31–37 kJ/mol, respectively. These findings indicate a direct correlation between the $k_{10}$ value and catalyst activity for the propane oxidation reaction, along with a direct relationship between the $k_{20}$ and $k_{30}$ values and the active site's propensity to form carbon oxides.

The kinetic parameters associated with the catalyst reoxidation reaction, $k_{40}$ and $E_4$, reveal that the $k_{40}$ values for the VMoTi catalysts followed the trend 2V2MoTi > 3.4V0.6MoTi > 0.6V3.4MoTi. The 0.6V3.4MoTi sample has the highest reoxidation activation energy (223 kJ/mol), followed by 2V2MoTi (159 kJ/mol) and then 3.4V0.6MoTi (119 kJ/mol).

Previous studies have suggested that the rate constant ratio, $k_1/(k_2 + k_3)$, is an important parameter to consider when comparing catalysts and determining operating conditions [32,34]. The variation in the $k_1/(k_2 + k_3)$ ratio for the different catalysts depends on the ratio of apparent pre-exponential factors, $k_{10}/(k_{20} + k_{30})$, and difference in activation energies, $\Delta E = E_1 - (E_2 + E_3)/2$ provided that $E_2$ and $E_3$ are similar. Values for the parameters $k_{10}/(k_{20} + k_{30})$ and $\Delta E$ also are given in Table 3. Because the $\Delta E$ values were relatively similar, the variation in the $k_1/(k_2 + k_3)$ values was similar to that in the $k_{10}/(k_{20} + k_{30})$ values; consequently, studying only the variation in the $k_{10}/(k_{20} + k_{30})$ ratio for the VMoTi catalysts is sufficient. Table 3 shows a trend in the $k_{10}/(k_{20} + k_{30})$ ratio of 3.42V0.6MoTi > 0.6V3.42MoTi > 2V2MoTi, consistent with the trend seen in experimental propene yields at iso-conversion.

Fig. 10 shows the predicted variations in propene yield with propane conversion based on the parameters estimated for the three VMoTi and 2VTi catalysts. The figure reveals that the trends in propene yield at iso-conversion are consistent with the trends seen in $k_1/(k_2 + k_3)$ values and are in accordance with the RSM analysis predictions. Furthermore, the varying $k_1/(k_2 + k_3)$ ratios with temperature shown in Fig. 11 indicate an increasing trend, because the difference in activation energies, $\Delta E = E_1 - (E_2 + E_3)/2$, is positive for these catalysts. Because the $k_1/(k_2 + k_3)$ ratio is related to the propene yield at iso-conversion, the increased $k_1/(k_2 + k_3)$ ratio with temperature also suggests an increase in alkene yield at iso-conversion [32]. Thus, the $k_1/(k_2 + k_3)$ or $k_{10}/(k_{20} + k_{30})$ values were directly linked to the propene yields at iso-conversion, as was expected from the analysis of a consecutive reaction [35].

To understand the effect of promotion of the VMoTi catalysts over the VTi catalysts in terms of kinetic parameters, it is worth comparing the kinetic parameters of the 2VTi and 2V2MoTi catalysts. Presence of molybdena in the 2VTi catalyst resulted in an increase in $k_{10}$ and because no change in $E_1$ was observed, an increase in $k_1$ as well. The increase in $k_1$ was reflected in the in-

crease in conversion. The presence of molybdena also increased the $k_{20}$ and $k_{30}$ values, along with (given similar $E_2$ and $E_3$ values) increased $k_2$ and $k_3$ values. But the increase in $k_1$ (or $k_{10}$) was much greater than that in $k_2+k_3$ (or $k_{20}+k_{30}$), and the important lumped parameter $k_1/(k_2+k_3)$ increased with the presence of Mo, resulting in increased propene yield at iso-conversion. Given the confirmed increase in $k_1/(k_2+k_3)$ from the addition of molybdena, the composition of vanadia and molybdena in the catalyst necessary to give the optimum propene yield can be determined. Furthermore, the most active catalyst in terms of conversion is that with the highest $k_1$ value. Based on its highest $k_1$ and $k_1/(k_2+k_3)$ values, the 3.42V0.6MoTi catalyst was determined to be the best catalyst for the molybdena-promoted vanadia–titania system.

## 6. Conclusion

Supported $V_2O_5$–$MoO_3/TiO_2$ (VMoTi) catalysts with different V and Mo loadings were prepared by the incipient wetness coimpregnation method. The monolayer surface coverage of (V + Mo) on titania support was assumed to be 6 wt%. Structurally, the addition of Mo to titania-supported vanadia did not lead to new mixed V–Mo or segregated oxide phases, but it did have a "crowding" effect on the surface oxide species that made them more polymerized. Our reaction data revealed that adding Mo to titania-supported vanadia catalysts modified the reaction parameters. It appears that the Mo addition can be tuned to titania-supported vanadia for optimum ODH performance. Based on this finding, the propane ODH reaction was carried out over these catalysts to examine the synergetic effect of vanadia and molybdena on propene yield. The optimum compositions of vanadia and molybdena required to achieve maximum yields were determined by applying the CCD of experiments and RSM. A full second-order model was fitted to the propene yield data using the foregoing methodology as a function of V and Mo. This model has been found to adequately describe the experimental range considered here. The maximum propene yields at iso-conversion were obtained for the VMoTi catalysts containing the highest V and lowest Mo concentrations (3.42V0.6MoTi) and the lowest V and highest Mo concentrations (0.6V3.42MoTi).

The kinetic parameters for the propane ODH reaction were successfully estimated for the foregoing optimum catalysts along with the design center catalyst (2V2MoTi) using a consecutive Mars–van Krevelen model. This reaction model considers propene to be a primary product and CO and $CO_2$ to be secondary products. The apparent pre-exponential factors of the VMoTi catalysts for propene formation ($k_{10}$) and for propene combustion ($k_{20}$ and $k_{30}$) were found to depend on the V and Mo composition and to follow the trend 3.42V0.6MoTi > 2V2MoTi > 0.6V3.42MoTi; however, the activation energy for propene formation, $E_1$, and propene combustion reactions, $E_2$ and $E_3$, were relatively independent of V and Mo loading. The $k_{10}$ value was directly related to the propane oxidation activity, and the $k_{20}$ and $k_{30}$ values were directly related to the propensity of the active site to form carbon oxides. Furthermore, the propene yield at iso-conversion correlated well with the rate constant ratio for propene formation to propene combustion reactions, $k_1/(k_2+k_3)$.

The promotional effect of the VMoTi catalysts over VTi catalysts was interpreted by comparing the kinetic parameters of the 2V2MoTi and 2VTi catalysts. Adding Mo to the 2VTi catalysts resulted in relatively similar activation energies for the propene formation and propene combustion reactions, along with an increase in the apparent pre-exponential factors for all of the reactions; however, the increase in $k_1$ (or $k_{10}$) was much greater than that in $(k_2+k_3)$ (or $k_{20}+k_{30}$), which in turn increased the $k_1/(k_2+k_3)$ ratio. This finding reflects a higher propene yield for the 2V2MoTi catalyst relative to the 2VTi catalyst. Thus, the 3.42V0.6MoTi catalyst was the promoted VMoTi catalyst with the highest activity ($k_1$) and propene yield at iso-conversion ($k_1/(k_2+k_3)$ ratio).

## Acknowledgments

The authors gratefully acknowledge the support from the Indian Department of Science and Technology. They thank D. Shee, IIT Kanpur, for assisting with the TPR experiments.

## Supplementary material

Supplementary material for this article may be found on SienceDirect, in the online version.

Please visit DOI: 10.1016/j.jcat.2008.07.001.

## References

[1] H.H. Kung, Adv. Catal. 40 (1995) 1.
[2] F. Cavani, F. Trifirò, Catal. Today 24 (1995) 307.
[3] E.A. Mamedov, V. Cortés-Corberan, Appl. Catal. A 127 (1995) 1.
[4] I.E. Wachs, B.M. Weckhuysen, Appl. Catal. A 157 (1997) 67.
[5] T. Blasco, J.M. López-Nieto, Appl. Catal. A 157 (1997) 117.
[6] K. Routray, K.R.S.K. Reddy, G. Deo, Appl. Catal. A 265 (2004) 103.
[7] A. Khodakov, B. Olthof, A.T. Bell, E. Iglesia, J. Catal. 181 (1999) 205.
[8] N. Boisdron, A. Monnier, L. Jalowiecki-Duhamel, Y. Barbaux, J. Chem. Soc. Faraday Trans. 91 (1995) 2899.
[9] R. Grabowski, S. Pietrzyk, J. Słoczynski, F. Genser, K. Wcisło, B. Grzybowska-Swierkosz, Appl. Catal. A 232 (2002) 277.
[10] R. Grabowski, J. Słoczynski, N.M. Grzesik, Appl. Catal. A 242 (2003) 297.
[11] A. Christodoulakis, M. Machli, A.A. Lemonidou, S. Boghosian, J. Catal. 222 (2004) 293.
[12] E. Heracleous, M. Machli, A.A. Lemonidou, I.A. Vasalos, J. Mol. Catal. A Chem. 232 (2005) 29.
[13] J.G. Eon, R. Olier, J.C. Volta, J. Catal. 145 (1994) 318.
[14] E.V. Kondratenko, M. Baerns, Appl. Catal. A 222 (2001) 133.
[15] A. Bottino, G. Capannelli, A. Comite, S. Storace, R.D. Felice, Chem. Eng. J. 94 (2003) 11.
[16] M.D. Argyle, K. Chen, A.T. Bell, E. Iglesia, J. Catal. 208 (2002) 139.
[17] A.A. Lemonidou, L. Nalbandian, I.A. Vasalos, Catal. Today 61 (2000) 333.
[18] N. Watanabe, W. Ueda, Ind. Eng. Chem. Res. 45 (2006) 607.
[19] I.E. Wachs, J.-M. Jehng, W. Ueda, J. Phys. Chem. B 109 (2005) 2275.
[20] P. Botella, J.M. López-Nieto, B. Solsona, A. Mifsud, F. Marquez, J. Catal. 209 (2002) 445.
[21] J.M. López-Nieto, R. Coenraads, A. Dejoz, M.I. Vazquez, in: R.K. Grasselli, S.T. Oyama, A.M. Gaffney, J.E. Lyons (Eds.), 3rd World Congress on Oxidation Catalysis, 1997, p. 443.
[22] P. Concepcion, P. Botella, J.M. López-Nieto, Appl. Catal. A 278 (2004) 45.
[23] G.G. Cortez, J.L.G. Fierro, M.A. Bañares, Catal. Today 78 (2003) 219.
[24] M.A. Bañares, S.J. Khatib, Catal. Today 96 (2004) 251.
[25] H. Dai, A.T. Bell, E. Iglesia, J. Catal. 221 (2004) 491.
[26] S. Yang, E. Iglesia, A.T. Bell, J. Phys. Chem. B 109 (2005) 8987.
[27] V. Ermini, E. Finocchio, S. Sechi, G. Busca, S. Rossini, Appl. Catal. A 198 (2000) 67.
[28] B. Mitra, I.E. Wachs, G. Deo, J. Catal. 240 (2006) 151.
[29] R. Grabowski, B. Grzybowska, K. Samson, J. Stoczynski, J. Stoch, K. Wcislo, Appl. Catal. A 125 (1995) 129.
[30] R. Grabowski, Appl. Catal. A 270 (2004) 37.
[31] D. Courcot, A. Ponchel, B. Grzybowska, Y. Barbaux, M. Rigole, M. Guelton, J.P. Bonnelle, Catal. Today 33 (1997) 109.
[32] R.P. Singh, M.A. Bañares, G. Deo, J. Catal. 233 (2005) 388.
[33] B.M. Weckhuysen, A.A. Verberckmoes, J. Debaere, K. Ooms, I. Langhans, R.A. Schoonheydt, J. Mol. Catal. A Chem. 151 (2000) 115.
[34] D. Shee, T.V.M. Rao, G. Deo, Catal. Today 118 (2006) 288.
[35] H.S. Fogler, Elements of Chemical Reaction Engineering, third ed., Prentice–Hall of India Pvt. Ltd., New Delhi, 2002.
[36] G.E.P. Box, K.G. Wilson, J. R. Stat. Soc. B 13 (1951) 1.
[37] D.C. Montgomery, Design and Analysis of Experiments, third ed., Wiley, USA, 1991.
[38] G.E.P. Box, J.S. Hunter, W.G. Hunter, Statistics for Experimenters, second ed., Wiley, USA, 2005.
[39] R.O. Kuehl, Design of Experiments: Statistical Principles of Research Design and Analysis, second ed., Duxbury, USA, 2000.
[40] I.E. Wachs, Catal. Today 27 (1996) 437.
[41] M.A. Vuurman, I.E. Wachs, A.M. Hirt, J. Phys. Chem. 95 (1991) 9928.
[42] G. Deo, I.E. Wachs, J. Catal. 146 (1994) 323.

[43] B.M. Weckhuysen, D.E. Keller, Catal. Today 78 (2003) 25.
[44] H. Hu, I.E. Wachs, S.R. Bare, J. Phys. Chem. 99 (1995) 10897.
[45] G. Tsilomelekis, A. Christodoulakis, S. Boghosian, Catal. Today 127 (2007) 139.
[46] K. Chen, A. Khodakov, J. Yang, A.T. Bell, E. Iglesia, J. Catal. 186 (1999) 325.
[47] T.V.M. Rao, G. Deo, Ind. Eng. Chem. Res. 46 (2007) 70.
[48] T.V.M. Rao, G. Deo, Catal. Commun. 8 (2007) 957.
[49] M.A. Bañares, I.E. Wachs, J. Raman Spectrosc. 33 (2002) 359.
[50] M.D. Amiridis, R.V. Duevel, I.E. Wachs, Appl. Catal. B 20 (1999) 111.
[51] N. Magg, B. Immaraporn, J.B. Giorgi, T. Schroeder, M. Bäumer, J. Döbler, Z. Wu, E. Kondratenko, M. Cherian, M. Baerns, P.C. Stair, J. Sauer, H.-J. Freund, J. Catal. 226 (2004) 88.
[52] S.J. Khatib, R. Guil-Lopez, M.A. Peña, J.L.G. Fierro, M.A. Bañares, Catal. Today 118 (2006) 353.
[53] G. Ramis, C. Cristiani, P. Forzatti, G. Busca, J. Catal. 124 (1990) 574.
[54] G. Busca, J.C. Lavalley, Spectrochim. Acta 42A (1986) 443.
[55] M. del Arco, C. Martin, V. Rives, V. Sanchez-Escribano, G. Ramis, G. Busca, V. Lorenzelli, P. Malet, J. Chem. Soc. Faraday Trans. 89 (1993) 1071.
[56] L. Lietti, I. Nova, G. Ramis, L. Dell'Acqua, G. Busca, E. Giamello, P. Forzatti, F. Bregani, J. Catal. 187 (1999) 419.
[57] M.A. Vuurman, D.J. Stufkens, Ad. Oskam, G. Deo, I.E. Wachs, J. Chem. Soc. Faraday Trans. 92 (1996) 3259.
[58] H.C. Yao, J. Catal. 70 (1981) 440.
[59] P. Arnoldy, J.C.M. de Jonge, J.A. Moulijn, J. Phys. Chem. 89 (1985) 4517.